Atom cooling in one dimension with high-intensity laser light

M. R. Williams, M. J. Bellanca, L. Liu, C. Xie, W. F. Buell,* T. H. Bergeman, and H. J. Metcalf
Department of Physics, State University of New York at Stony Brook, Stony Brook, New York 11794-3800
(Received 26 December 1996; revised manuscript received 12 May 1997)

In sub-Doppler laser cooling of atoms, the lowest temperatures are known to occur at low (but not too low) excitation, and the temperature increases roughly linearly with laser intensity. However, under conditions for which the lowest temperatures are obtained, the small velocity capture range and low optical pumping rate limit the number of atoms that can be collected into the cold sample. In this study, we present measurements for laser cooling of Rb and metastable He atoms for two counterpropagating laser beams with orthogonal linear polarization (lin⊥lin) over a wide range of saturation parameters and laser detunings, together with results of semiclassical (Fokker-Planck) and quantum density matrix calculations. We find that at higher laser intensity, a larger number of atoms can be collected into a final velocity distribution that is significantly narrower than that given by a linear extrapolation vs the square root of laser intensity. Two cooling mechanisms are at work: the sub-Doppler Sisyphus mechanism and also Doppler cooling. Under certain conditions that we discuss, Doppler cooling aids Sisyphus cooling by collecting high-velocity atoms beyond the Sisyphus capture range. He* presents a rather unusual situation in that the minimum average kinetic energy (E_{av}) for purely Sisyphus cooling is comparable to the minimum value of E_{av} with Doppler cooling alone. [S1050-2947(98)00501-0]

PACS number(s): 32.80.Pj, 42.50.Vk

I. INTRODUCTION

Optical collimation to produce the brightest atomic beams is important in many experimental situations, including atomic beam lithography and experiments in collisions and spectroscopy. To optimize atomic beam intensity and collimation simultaneously, one needs to balance the conditions for the narrowest velocity distributions against the conditions for efficient collection of atoms into a small range of velocities. The resultant ''cold peak'' in the velocity distribution at $v=0$ corresponds to a low temperature when it has a Gaussian shape. Polarization gradient and other sub-Doppler cooling methods depend on the multilevel structure of atoms to achieve temperatures lower than with purely Doppler cooling, but the velocity capture range of such methods is quite restricted. Still lower temperatures have been achieved by velocity selective coherent population trapping [1–3], but this alone does not efficiently collect fast atoms into the cold peak [4]. The lowest reported temperatures have been achieved by evaporative cooling in three dimensions [5–7], but this technique cannot be used for brightening of atomic beams.

Recently it has been reported that there is an unexpectedly small increase in the width of the velocity distribution when high-intensity light is used to collimate atomic beams in a one-dimensional lin⊥lin configuration [8–10] (lin⊥lin laser cooling employs counterpropagating laser beams with orthogonal linear polarization). This conclusion is most explicit in the work with Rb and Na atoms [8,9], but was also reported with Cr [10]. In view of these results, our goal has been to obtain additional data for Rb and also to study lin⊥lin cooling of metastable He atoms (He*), and to compare our measurements with theoretical models that were not available for the Na and Cr studies in order to better understand laser cooling under these conditions.

We find that at high intensity for Rb, and moderate intensity for He*, Doppler cooling and polarization gradient (Sisyphus) cooling complement each other, resulting in a larger velocity capture range while maintaining a relatively narrow final width in the velocity distribution. Each of these cases lies outside the region of applicability of models in which the excited state populations are adiabatically eliminated (AE) [11–14]. The measured widths of the velocity distributions turn out to be significantly narrower than would be found from extrapolation to higher intensity of AE results such as those in [12,14]. Our calculations, using both quantum density matrix and semiclassical Fokker-Planck equation methods with excited states retained, show that deviations from an overall Gaussian velocity distribution play an important role. As previously recognized [12], non-Gaussian distributions are ubiquitous in lin⊥lin cooling.

The non-Gaussian character can be understood by considering the velocity dependence of both the semiclassical force $[F(v)]$ and momentum diffusion $[D(v)]$ functions [12,15–17]. The steady-state velocity distribution $[P(v)]$ calculated from the Fokker-Planck equation is Gaussian when the ratio $F(v)/D(v)$ is linear in v. Ideally [12] one has $F(v) \propto v/[1+(v/v_c)^2]$, where v_c is the velocity capture range, and $D(v)=D_1/[1+(v/v_c)^2]+D_0$, in which D_0 is negligible. In such a case, $F(v)/D(v) \propto v$ everywhere. Since $F(v)$ and $D(v)$ are useful tools for qualitative (and nearly quantitative) understanding of the experimental results, we have developed a semiclassical algorithm for calculating $F(v)$ and $D(v)$ that includes excited states [16–18], and present some of these results below. In the results from these semiclassical calculations of $D(v)$, D_0 is typically not negligible for $v > v_c$, and in fact $F(v)$ and $D(v)$ do not exactly follow the above simple parametrizations. As a consequence, even at low intensity and large detuning, we find that the linear region of $F(v)/D(v)$ typically does not extend significantly

*Present address: The Aerospace Corporation, Mailstop M2/253, P.O. Box 92957, Los Angeles, CA 90009-2957.

beyond the maxima of $|F(v)|$ at $v=\pm v_c$. Since $P(v)$ normally *is* significant beyond $v=v_c$, there are usually more atoms in the wings than for a truly Gaussian shape, and one can say that lin⊥lin cooling is typically less efficient for larger $|v|$. Thus $E_{\rm av}\equiv M\langle v^2\rangle/2$ is often greater than the estimate $E_{ge}=Mv_{ge}^2/2$, where v_{ge} is the $1/\sqrt{e}$ half-width of the velocity distribution, or $E'_{ge}=M(\Delta v)^2/8\ln 2$, where Δv is the full width at half maximum (FWHM) of $P(v)$. [For Gaussian $P(v)$, $E_{\rm av}=E_{ge}=E'_{ge}$.] $E_{\rm av}$ is strongly influenced by Doppler cooling, which collects atoms from the wings into the cold atom peak.

Better agreement with the measurements can be obtained with quantum density matrix or quantum Monte Carlo calculations than with such semiclassical methods, especially for ground state $F>1$. In this study we use two quantum density matrix methods. Time evolution calculations with a basis of free-particle states (labeled ''QDM'' here) include excited states and are believed to be most accurate. The quantum basis states for AE calculations are the eigenstates in the light shift potential, obtained by eliminating the excited states. *Steady-state* AE results depend only on the parameter U_0/E_r, and not otherwise on the detuning or intensity [13]. Here $U_0=-f\hbar\delta S/(1+4\delta^2/\Gamma^2)$ is the depth of the optical potential wells, $f\equiv[(F+1)(2F+1)-1]/[(F+1)(2F+1)]$, $\delta=\omega_L-\omega_A$ is the detuning of the laser frequency ω_L from the atomic resonance frequency ω_A, and $\Gamma=1/\tau$ is the spontaneous emission rate. $S\equiv I/I_{\rm sat}$ is the saturation parameter, where $I_{\rm sat}\equiv\pi hc/3\lambda^3\tau$, $E_r\equiv Mv_r^2/2$ is the recoil energy for an atom of mass M cooled on a transition of wavelength $\lambda=2\pi/k$, and $v_r=\hbar k/M$ is the recoil velocity. The excited state fraction is related to the ratio Γ_p/Γ, where $\Gamma_p\equiv S\Gamma/2[1+S+(2\delta/\Gamma)^2]$. For a two-level atom, rate equations give the excited state fraction to be $\Gamma_p/(2\Gamma_p+\Gamma)$, and this is approximately true also for lin⊥lin excitation of a multilevel atomic transition, although different branches and Clebsch-Gordan factors modify this result. AE is valid when $\Gamma_p\ll\Gamma/2$. Within the AE approximation, the minimum value of $E_{\rm av}$ in lin⊥lin cooling occurs at $U_0/E_r\approx 100$ [12]. For $U_0/E_r\gtrsim 100$, steady-state AE calculations show that $E_{\rm av}$ increases approximately linearly with U_0/E_r or with S, hence the FWHM of $P(v)$ increases roughly as $S^{1/2}$.

Some of the Rb experiments reported here, however, go beyond the regime where the FWHM of $P(v)$ is a linear function of $S^{1/2}$. For detuning $|\delta|<5\Gamma$ and at higher values of U_0/E_r, we find that $P(v)$ is narrower than the width extrapolated from low-intensity results, as found also in three-dimensional (3D) laser cooling experiments [19]. This narrowing occurs largely because Sisyphus cooling is assisted by Doppler cooling at large $|v|$, especially at high laser intensity. Such assistance not only helps to narrow $P(v)$, but more importantly, also collects high-velocity atoms from the wings. We emphasize that Doppler cooling effects are obtained theoretically only when excited states are included in the calculation, and thus do *not* appear in AE calculations.

The role of Doppler cooling relative to Sisyphus cooling depends on $\varepsilon\equiv E_r/\hbar\Gamma=\hbar k^2/2M\Gamma$. For lin⊥lin cooling, the minimum $E_{\rm av}$ varies from about $45E_r$ for $F=1/2\rightarrow 3/2$ to $20E_r$ for $F=3\rightarrow 4$ transitions. The 1D Doppler cooling limit is $E_{\rm av}=\langle Mv^2/2\rangle=kT_{\rm min}/2=7\hbar\Gamma/40$ [20,21]. When translated into units of E_r, the Doppler limit can vary greatly between different atoms, and thus the strategy for optimizing the capture velocity and the width of $P(v)$ depends on ε.

Experiments with He* cooled on the $2\,^3S_1\rightarrow 2\,^3P_2$ transition at $\lambda=1.083\ \mu$m present an interesting contrast with Rb because ε is larger ($\varepsilon=2.6\times10^{-2}$ for He*, vs 6.4×10^{-4} for Rb) [22]. Thus while the Doppler limit for Rb is $273E_r$, it is only $6.7E_r$ for He*, or about one-fourth of the Sisyphus limit, $E_{\rm av}=25E_r$. An important difference between Sisyphus and Doppler cooling is in the behavior at relatively large velocities. First, the velocity capture range v_c, given approximately by one-half the separation between the peaks in the $F(v)$ functions, is typically larger for Doppler cooling than for Sisyphus cooling. For Doppler cooling, $v_c\approx|\delta|/k$, while for lin⊥lin Sisyphus cooling, $v_c=\overline{f}\,\Gamma_p/k$, where $\overline{f}=2/9$ for a $F=1/2\rightarrow 3/2$ transition at low intensity [11] and comparable values for other F_g as given in Sec. IV C. [See Ref. [23] for plots of $F(v)$ vs scaled velocity for various F_g at one particular detuning value.] Secondly, at less than optimum values of U_0/E_r, the velocity diffusion rate in the wings produces a sharp rise in $E_{\rm av}$, as seen in AE results reported in [12] and presented here. This is associated with the velocity-independent term in $D(v)$ (D_0 in the notation of Ref. [12]), and is due to fluctuations in the difference of the momentum carried away by the two counterpropagating laser beams. However Doppler cooling continues to function in this regime. Quantum density matrix (QDM) results show that for He*, if the detuning is not too large (see Sec. IV C), Doppler cooling removes the sharp increase in $E_{\rm av}$ at small U_0/E_r. Although we do not measure $E_{\rm av}$ in He*, we clearly observe non-Gaussian velocity distributions that arise because the linear range of $F(v)/D(v)$ is small relative to the steady-state velocity FWHM.

The organization of this paper is as follows. In Sec. II we give a brief description of our semiclassical and quantum density matrix methods. Also in this section, results of semiclassical calculations show how high laser intensity can be used to collect atoms from a large velocity range into a relatively narrow cold peak. In Sec. III we describe our experimental setups for Rb and He* and the methods of data analysis. In Sec. IV we compare experimental results with computations performed with both semiclassical Fokker-Planck and quantum density matrix methods. In Sec. V we discuss implications of these and other similar results. Both the theoretical and experimental work reported here are restricted to one dimension.

II. THEORY

We have employed both semiclassical Fokker-Planck equation (SC-FPE) and quantum density matrix methods to calculate atomic velocity distributions. The SC-FPE method [12,15,16,18] is efficient, versatile, and gives useful physical insight through the calculated $F(v)$ and $D(v)$, in spite of certain limitations we describe below. We have formulated the equations and a computer algorithm to compute both $F(v)$ and $D(v)$ in 1D for multilevel atomic transitions including excited state levels [16]. Our method parallels that used by Berg-Sørensen *et al.* [15] for cooling of two-level atoms. To obtain the steady-state density matrix elements for

the various internal states at a given velocity, we use a continued fraction method [24] differing slightly from that used in Ref. [15] to avoid singular matrices that occur with multilevel atoms. Because of the high saturation parameters involved in this work, it was necessary to go to high order (up to 180) in the continued fraction computations. For computational efficiency, we have exploited the block matrix substructure of the evolution matrix.

Given $F(v)$ and $D(v)$, the steady-state velocity distribution $P(v)$ can be obtained by simple integration:

$$P(v)=N\ \exp\left[\int_{-\infty}^{v} dv' F(v')/D(v')\right], \tag{1}$$

where N is a normalizing coefficient. The time evolution can be obtained from the FPE for the momentum distribution $W(p)$:

$$\frac{dW(p)}{dt}=-\frac{\partial}{\partial p}[F(p)W(p)]+\frac{\partial}{\partial p}\left(D_{\rm st}(p)\frac{\partial}{\partial p}W(p)\right) + \frac{\partial^2}{\partial p^2}[D_{\rm sp}(p)W(p)], \tag{2}$$

where $p=Mv$, and $D_{\rm st}(p)$ and $D_{\rm sp}(p)$ are the contributions to the diffusion from stimulated and spontaneous emission, respectively. The derivation of this form [16] follows from a generalization of the treatment of Minogin [25]. Several other authors have employed the form of Eq. (2), e.g., [26,27]. Other forms of the FPE for laser cooling have been used elsewhere [15,28].

Figure 1 shows plots of $F(v)$ and $D(v)\equiv D_{\rm st}(v)+D_{\rm sp}(v)$ for lin⊥lin cooling on the ^{85}Rb $F=3\rightarrow 4$ transition. Figure 1(a) is for $S=1.5$, $\delta=-5\Gamma$, hence $U_0/E_r=110$, and shows a steep gradient in $F(v)$ near $v=0$. Figure 1(b) (for $S=20$, $\delta=-5\Gamma$) shows that at higher S, the velocity range over which the force is significant is larger than in Fig. 1(a), while in Fig. 1(c) ($S=20$, $\delta=-\Gamma$), the force remains substantial over the entire velocity range shown, albeit with a smaller gradient at the origin.

These functions are used together with Eq. (2) to calculate the time evolution of the velocity distribution as shown in Fig. 2 [(a), (b), and (c) correspond to the respective parts of Fig. 1]. The interaction times in Fig. 2 extend up to 1000τ, or about 27 μs, and the initial velocity distribution is taken to be flat out to $\pm 180 v_r = 1.08$ m/s, as in our experiments. The conditions of Fig. 2(a) give a velocity peak with nearly the minimum width, but only a small fraction of the atoms are collected into it. In (b) the cold peak is somewhat wider than in (a), but many more atoms are collected. By reducing the detuning to $\delta=-\Gamma$ as in Fig. 2(c), virtually all the atoms are collected into the cold peak even after an interaction time of only 1000τ. These computational results illustrate the possibilities for obtaining increased atomic beam intensities by collimation with intense laser light and small detunings. Calculations in this last regime of S and δ have generally not been done previously because the simplifying assumption of AE is no longer valid.

Clearly, the cases shown in Figs. 1 and 2 do not provide a systematic survey of results expected under various condi-

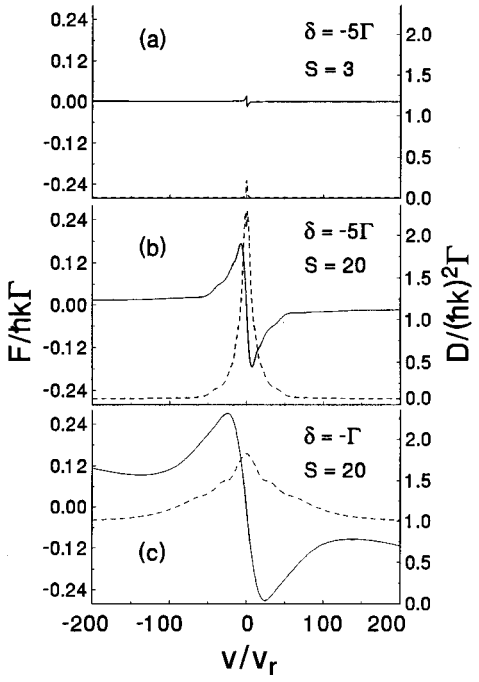

FIG. 1. Velocity-dependent semiclassical force and diffusion functions for the ^{85}Rb $F=3\rightarrow 4$ transition for different choices of the laser parameters. (a) $S=1.5$, $\delta=-5\Gamma$ (optimum U_0/E_r) leads to a large damping rate over only a very small range of velocities. (b) $S=20$, $\delta=-5\Gamma$ leads to a much larger capture range. (c) $S=20$, $\delta=-\Gamma$ results in a slowing force over the entire velocity range under consideration.

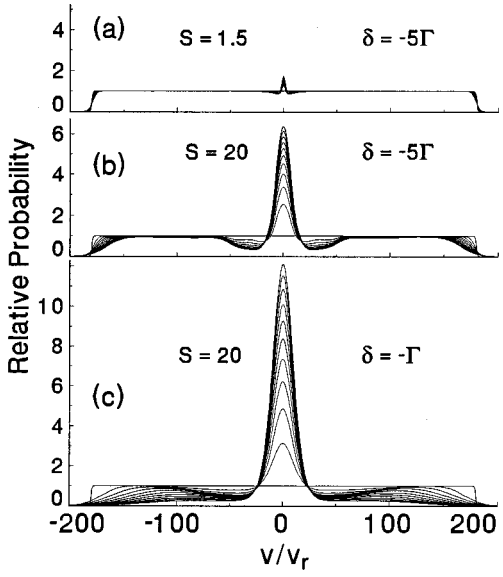

FIG. 2. Temporal evolution of velocity distributions for different choices of laser parameters in intervals of 100τ. The laser parameters correspond to those of Fig. 1. (a) shows a very narrow cold peak because of the large damping constant, but the narrow velocity capture range leaves most of the initial distribution uncooled. (b) leads to a somewhat wider cold peak, but with many more atoms collected into it. (c) collects virtually all the atoms into a respectably narrow cold peak.

tions of detuning and intensity. Optimum conditions for collecting atoms will depend on the atomic species, the available interaction time, the available laser intensity, and the initial range of velocities. Furthermore, equilibration to a cooler velocity distribution in a region of decreasing laser intensity [29] offers possibilities for attaining a narrower $P(v)$ once the atoms have been collected into a cold peak with intense laser light. Thus the combination of high-intensity collimation techniques discussed here with low-intensity cooling in the tail of the laser spatial distribution and with other techniques mentioned in Ref. [30] and in Sec. V has promise for producing very bright atomic beams.

The QDM method [13, 14, 22, 31] offers a more quantitative computational approach using a basis of direct products of momentum eigenfunctions and internal states, $|p,m\rangle = |p\rangle \otimes |m\rangle$, including excited states. The Hamiltonian for this calculation includes the atomic center of mass motion, the internal atomic energy levels, and the atom-laser interaction [22,31].

Because of the wide initial velocity range and the number of internal states for the $F=3\rightarrow 4$ transition, we have not attempted detailed modeling of the time evolution for the ^{85}Rb experiment with QDM calculations. However, we have used QDM calculations to determine steady-state $P(v)$ by starting with a velocity distribution nearly equal in width to the final one. For such calculations, we used 80–160 momentum states for each of 16 internal m_F states, resulting in a total of $\mathcal{N}=1300-2600$ basis states. The density matrix included only those off-diagonal elements between states connected by the atom-laser interaction (within ''families''), and within a limited range of momentum differences. Typically, there were $\mathcal{N}^2/20$ elements of the density matrix used in the calculations. The results of the calculations are shown in later sections in comparison with our measurements. For the He* $J=1\rightarrow 2$ transition, the number of internal states and momentum basis states was small enough that we could use the QDM method to model the temporal evolution of the cooling process, including the spatial variation of the laser profile.

III. EXPERIMENTAL APPARATUS AND DATA REDUCTION

A. Rubidium

Our apparatus for Rb is shown in Fig. 3. A thermal atomic beam is produced by an oven operated at $T=450$ K with a horizontal 2 mm$\times$100 μm slit, and the beam is defined by a vertical 25 μm$\times$2 mm collimation slit 34 cm downstream. This configuration results in an initial transverse velocity full width of about $350v_r$. The atomic beam crosses counterpropagating laser beams of orthogonal linear polarizations from a Ti:sapphire laser in a 3 cm long interaction region where the magnetic field has been canceled to better than ± 5 mG.

To compensate the effects of optical hyperfine pumping in ^{85}Rb, phase modulation sidebands are applied by an electro-optic modulator at a frequency of $\omega_{\rm sb}=\Delta_g-\Delta_e+\delta$, where $\Delta_g/2\pi=3.036$ GHz is the ground state hyperfine splitting and $\Delta_e/2\pi=120$ MHz is the excited state hyperfine splitting between $F_e=3$ and 4. The sidebands are adjusted so that $S_{\rm sb}\approx 1\%$ of the main carrier, although the results are generally insensitive to details of this repumping intensity. The laser beam profile is nearly an elliptical Gaussian with a beam diameter ($1/e^2$) along the atomic beam direction of 20 mm and truncated to a diameter of 10.4 mm. Further, the downstream edge of the beam has been chosen to be where the intensity is about 85% of the maximum to minimize effects of low-intensity cooling as atoms exit the interaction region [29] (See inset to Fig. 3.) We position the cutoff aperture as close as possible (about 10 cm) to the interaction region to minimize the effects of diffraction fringes.

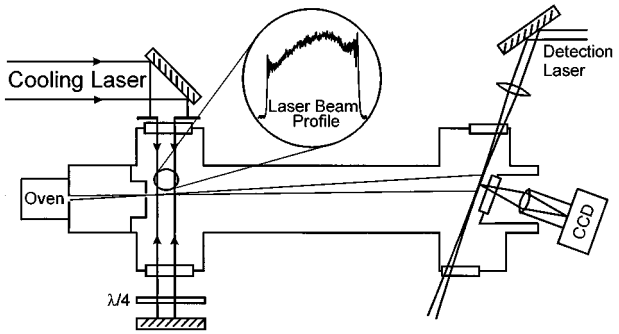

FIG. 3. Apparatus for Rb experiments showing the thermal atomic beam geometry and the sheet of light fluorescence detection scheme arranged for velocity selective detection with the detection laser at an angle of 110° with respect to the atomic beam. The inset shows the measured cooling laser beam spatial profile.

A part of the cooling laser beam is split off and passes through an acousto-optic modulator (AOM) with a center frequency of 80 MHz, and the down-shifted beam is used in a standard saturated absorption spectroscopy arrangement. The laser frequency is thereby locked by saturated absorption spectroscopy near the $5\ ^2S_{1/2}(F_g=3)\rightarrow 5\ ^2P_{3/2}(F_e=4)$ transition (of ^{85}Rb), either to a Lamb dip or a crossover resonance. By locking to appropriate lines and using different AOM frequencies, we can achieve a wide range of detunings for the cooling laser beam. The absolute uncertainty in the laser intensity was about 10% (measured with a photodiode calibrated with a thermopile detector), but the relative uncertainty (i.e., fluctuation) was only 2%.

The resulting atomic velocity distribution is measured 1.6 m downstream using fluorescence detection with a charge-coupled device (CCD) camera as the atoms traverse a resonant sheet of light. The detection laser beam is produced by a linewidth narrowed ($\delta\nu_L<1$ MHz), grating feedback diode laser [33] (Sharp LTO25) operated in the weak feedback regime for spectral narrowing. The beam power is attenuated to 1.4 mW and is focused in one dimension by cylindrical optics into a sheet of light with a waist size of 50 μm$\times$1 cm. This beam intersects the atomic beam and the resulting fluorescence is imaged with 1:1 magnification onto a thermoelectrically cooled CCD detector array. Because the laser cooling geometry is basically one dimensional, we sum the pixels vertically over a length of 1700 μm. The spatial resolution of the detection system is 11.5 μm, resulting in a detection resolution of $0.4v_r$ for a longitudinal velocity of $v_L=\sqrt{3k_BT/M}\approx 360$ m/s. However, the 25 μm collimating slit introduces a spatial averaging that makes the effective velocity resolution about equal to v_r.

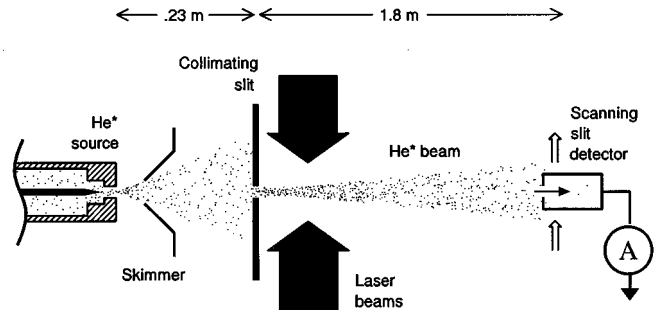

FIG. 4. Schematic of apparatus for He* experiments, showing atomic beam geometry and metastable atom detection region.

This detection mechanism is clearly state and isotope selective. We make it velocity selective as well by choosing the angle between the detection laser and the atomic beams to be other than 90°. For our velocity selective detection we set this angle to be 110° and choose the detuning of the detection laser to be resonant with a particular longitudinal velocity class so that we can selectively detect only a slice of the longitudinal velocity distribution. For our parameters, the width of the selected velocity class was approximately 50 m/s. This has two advantages: all detected atoms have had approximately the same laser-atom interaction time, and there is little spreading in the transverse velocity measurement from a variation in the times of flight.

The raw data from the CCD have been processed in two steps to minimize the effects of background scattered light and to normalize for variations in the atom beam flux. First, an image taken with the sheet-of-light detection laser tuned very far above resonance was subtracted from it. Second, this difference was divided by a polynomial that was fit to a measured profile obtained with the cooling laser beam blocked, after a similar subtraction. The major sources of background are scattered light from the detection laser, scattered light from the cooling laser, and fluorescence from the interaction region. (There remains a very small amount of scattered light signal from rescattered fluorescent light in the detector region that is not accounted for in this procedure.) In the absence of any cooling this procedure would produce a flat line at 1. By translating the atomic beam, we estimate that the initial velocity distribution is flat to within about 20% out to $\pm 180 v_r$.

B. Helium

In order to eliminate concerns about hyperfine optical pumping and, more importantly, to elucidate features particular to lighter atoms, we have performed experiments in ^{4}He* to complement our results in Rb. The apparatus for the He* experiment has been described in [34] and will be briefly reviewed here (see Fig. 4.) A supersonic beam of He* atoms is produced in a liquid-nitrogen cooled, discharge-excited source. With our standard operating conditions, the longitudinal velocity distribution is centered at 1600 m/s and is approximately 240 m/s wide. The source output is approximately 5×10^{13}(He* atoms) s^{-1} sr^{-1}, and the ratio of $2\,^1S$ to $2\,^3S$ metastable atoms is less than 0.02. The flux through a 35 μm$\times$6 mm vertical collimation slit located 25 cm downstream from the nozzle is 2×10^8 atoms/s. The magnetic field in the interaction region is zeroed to ± 5 mG with three pairs of Helmholtz coils.

Immediately after the slit the atoms pass through two equal intensity, counterpropagating laser beams produced by a laser-diode pumped cw lanthanum neodymium hexaaluminate (LNA) laser operating at $\lambda = 1.083$ μm [35]. Along the atomic beam (longitudinal) direction, the laser beams have a $1/e^2$ full width of 16 mm and are apertured to 32 mm. For some measurements the laser beam is blocked 20.5 mm downstream of the slit with a straight edge, so that it is cut off downstream of the Gaussian peak at 85% of the maximum laser intensity. Thus the atoms are prevented from equilibrating to a narrower velocity distribution in the low-intensity Gaussian tail of the laser spatial profile. As in the Rb experiments, care is taken to minimize diffraction effects in the cutoff beam. In other scans the atoms are affected by the entire 32 mm of the apertured Gaussian laser beam width allowing further cooling in the low-intensity tail.

After the interaction region, the atoms travel 1.7 m to the detector. A 30 μm slit in front of the movable detector limits the transverse velocity resolution to 4.4 cm/s or $0.5 v_r$. The metastable He* atoms are detected by conversion electron emission when they strike a stainless steel plate in the detector. The liberated electrons are accelerated to a pair of microchannel plates, and the resulting current read by a picoammeter whose output is fed to the computer.

Since the detection mechanism for He* is different from that for Rb, the backgrounds and hence data analysis are different. The measured velocity profiles show the cooled velocity distribution of metastable atoms minus a background scan. The background is taken by increasing the He source pressure to collisionally quench the metastable atoms so that only the ultraviolet light from the discharge produces photoelectrons at the conversion surface of the detector. Thus the difference of the signal and background scans for an experiment with the laser blocked simply records the initial atomic velocity distribution.

IV. EXPERIMENTAL RESULTS AND COMPARISON WITH THEORY

A. Results with Rb atoms—flat initial velocity distribution

Examples of the transverse velocity distribution of Rb atoms obtained from CCD exposures are shown in Fig. 5. The asymmetry that appears in the observed $P(v)$ at high laser intensity probably arises from a slight imbalance in the laser cooling beams, particularly in the tail of the intensity distribution, where the edge of the reflected beam is somewhat smeared by diffraction effects. For the fitted curves in Fig. 5, we have simulated this effect by introducing different baseline slope parameters on either side of the velocity peak.

For Rb, we summarize the data from the individual CCD exposures by plots of the FWHM of the velocity distribution versus $S^{1/2}$. Typically, it is not possible to determine $E_{\rm av} = M\langle v^2\rangle/2$ accurately from measurements because $E_{\rm av}$ is very sensitive to the baseline, which often is not well determined. By contrast, the full width at half maximum is not so strongly affected by the baseline, and this is typically the relevant measure for the velocity range where the bulk of the atoms lie. The FWHM values extracted from fits to the CCD exposures have been plotted vs $S^{1/2}$ in Figs. 6(a) and 6(b) for

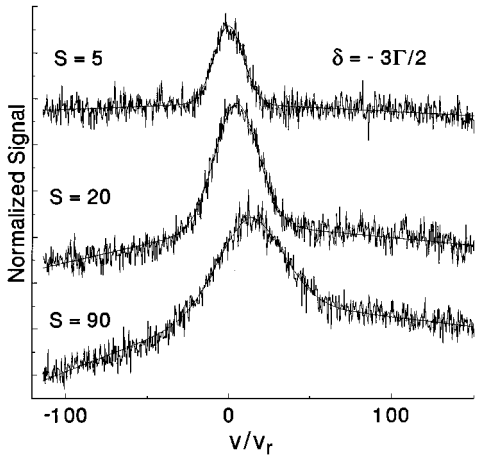

FIG. 5. Measured Rb atomic beam fluorescence profiles for detuning $\delta=-3\Gamma/2$ and for three values of the saturation parameter S. These data were taken for longitudinal velocity class $\overline{v_L}=350$ m/s. See text for the normalization or background subtraction procedure.

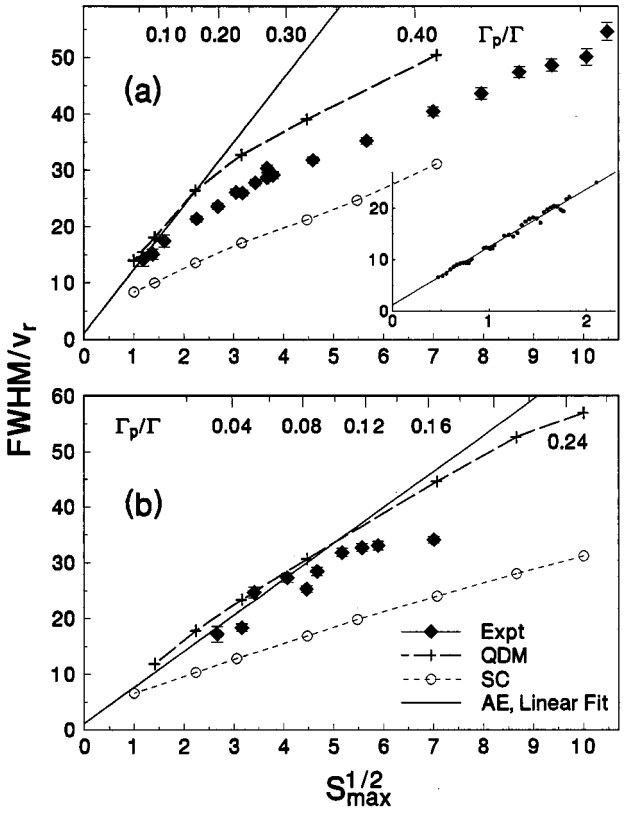

FIG. 6. FWHM of the ^{85}Rb atomic velocity distribution vs $S^{1/2}$ for laser detunings (a) $\delta=-3\Gamma/2$ and (b) $\delta=-5\Gamma$. The experimental FWHM values (diamonds with error bars) are taken from fits to the measured distributions as shown in Fig. 5. Also shown are results of SC-FPE (open circles) and QDM calculations (plus signs), as well as a linear fit (straight solid lines) to the low-intensity AE results for $F=3\rightarrow4$. The inset in (a) shows the computational data points and the fitted line. The small dips represent resonance transfer processes, as discussed by Courtois [36] for the case of $F=4\rightarrow5$. The scale at the top of each figure gives Γ_p/Γ, from which an estimate of the excited state fraction can be obtained as discussed in the text.

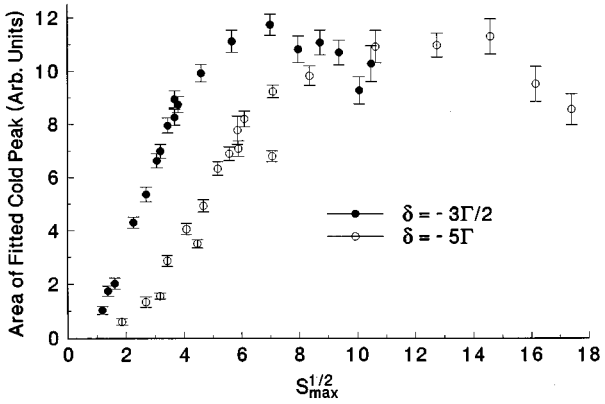

FIG. 7. Plot of the area under the Rb cold peak (fit height times fit width) vs $S^{1/2}$ for detunings $\delta=-3\Gamma/2$ and $\delta=-5\Gamma$. The area reaches a plateau when essentially all of the atoms are collected into the cold peak.

detunings $\delta=-3\Gamma/2$ and -5Γ, respectively. These figures also show FWHM values obtained from SC-FPE and steady-state QDM calculations.

At low intensities the FWHM increases roughly linearly with $S^{1/2}$. The solid lines in Fig. 6 are obtained from a linear fit to AE results at lower values of $S^{1/2}$, as shown explicitly in the inset to Fig. 6(a). At low intensities there is good agreement between AE and QDM results. By contrast, Figs. 6(a) and 6(b) indicate that the measured and also the calculated FWHM values at high intensity are less than expected from these linear extrapolations of the low-intensity calculations. For both $\delta=-3\Gamma/2$ [Fig. 6(a)] and $\delta=-5\Gamma$ [Fig. 6(b)], the deviations start to be significant when Γ_p/Γ is approximately 0.2 (the excited state fraction is about 0.15) as shown by the top scale in each part of Fig. 6. For given laser intensity, as detuning increases, Γ_p/Γ decreases and, accordingly, the deviations decrease.

A second parameter of interest here, in addition to the FWHM of the velocity distribution, is the number of atoms in the cold peak, as indicated by its area. Figure 7 shows that this area (fit amplitude times fit width) for both detunings does increase approximately linearly with $S^{1/2}$, up to the regime where almost all the atoms have been captured into the cold peak (giving an area of about 11 units in this figure). The combination of plots such as Figs. 6(a) or 6(b) and 7 indicate that over a range of S in which the FWHM doubles, the number of atoms within the cold peak increases tenfold. Such plots can be used to select the optimum laser detuning and intensity.

The discrepancies between experiment and QDM results shown in Fig. 6, especially at high laser intensity, may be associated with some degree of equilibration to a narrower velocity distribution in the low-intensity tail of the laser spatial profile. Furthermore, the plotted S values refer to the maximum of a Gaussian that was cut off downstream at approximately 85% of the maximum. The SC-FPE results in Fig. 6 show distinctly lower FWHM values than the experimental values or the QDM results. Since it is plausible that experimental widths would be narrower than theory, there is no reason to doubt that the QDM results are more accurate. Therefore the question arises why SC-FPE calculations are inaccurate.

We find that the discrepancies between QDM and SC-FPE results are much smaller for laser cooling on an $F=1/2\rightarrow 3/2$ or $F=1\rightarrow 2$ transition. We believe that the good agreement for $F_g=1/2$ and 1 validates our computer algorithms, including such effects as transfer of coherences from excited to ground states in spontaneous decay, which occurs for $F_g \geq 1$. We do not fully understand the origin of the discrepancies between SC-FPE and QDM steady-state results for $F_g>1$. Factors neglected in the SC-FPE approach are (a) the spatial dependence of $F(v,x)$ and $D(v,x)$ on a wavelength scale, (b) effects of the atomic deBroglie wavelength necessarily neglected in any SC method, and (c) correlation time effects (the Fokker-Planck equation assumes that diffusion processes act with a δ-function time correlation [37,38]).

We have used a semiclassical Langevin method [39] that *included* spatial dependence in $F(v,x)$ and $D(v,x)$ for two-level (Doppler) cooling processes, and found that it removes a large part of the discrepancies between QDM and SC results for this simpler situation [22]. For lin$\perp$lin Sisyphus cooling, it is not clear why spatial effects would be larger for $F=3\rightarrow 4$ transitions than for $F=1\rightarrow 2$ transitions. However, for larger F, there is a much wider range of values of the Clebsch-Gordan coefficients. The redistribution of population among m_F levels as an atom moves through the laser standing wave may not be rapid compared with the damping time. If this affects only the correlation time (which is assumed to be infinitesimal with the Fokker-Planck equation), it appears to act in the wrong direction. Preliminary results [39] with the Langevin equation approach to two-level cooling indicate that longer correlation times tend to *narrow* the velocity distribution. If this conclusion applies to lin$\perp$lin cooling, it would increase the discrepancy between SC and QDM results. Further studies of spatial dependence in semiclassical calculations are complicated by the tendency of $D(v,x)$ to go negative over part of the spatial period. Thus the reasons for the apparent failure of the SC-FPE approach for $F_g>1$ remain an unsolved problem.

B. Results with Rb atoms—narrow initial distribution at nonzero velocity

We now turn our attention to the manner in which atoms at high transverse velocities are collected into the cold peak. To study the dynamics of the deceleration of atoms with high transverse velocities, we prepared the atoms in an initial distribution of width approximately $40v_r$ centered at $v=180v_r$ by using parallel collimating slits. We then took CCD exposures of the cooled distribution for a series of interaction times by increasing the interaction length symmetrically about the peak of the Gaussian laser profile. Figure 8 shows such traces together with calculations using the SC-FPE approach. This figure illustrates several quite interesting aspects of the collection dynamics of high-velocity atoms into the cold peak. At short times the high-velocity atoms are decelerated by the Doppler force, which has a large capture range, but at the same time, diffusion broadens the velocity distribution considerably. When atomic velocities are within the capture range of the Sisyphus cooling force, these atoms are captured into the cold peak.

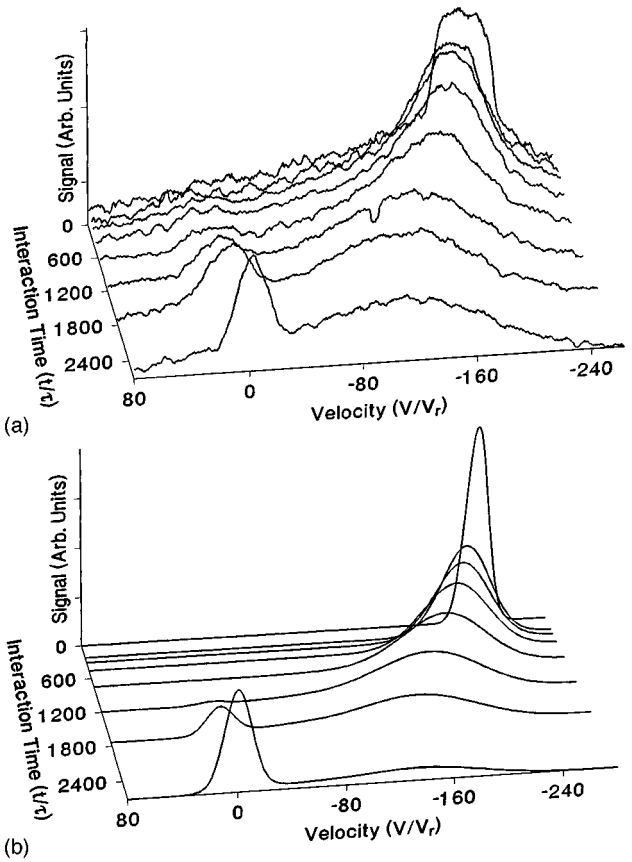

FIG. 8. Dynamics of the collection of high-velocity Rb atoms into cold peak: (a) experimental results and (b) SC-FPE calculation. In both the experiment and the calculation, the initial distribution is taken to be a peak $40\hbar k$ wide centered at $v=180v_r$. The laser parameters are $S=30$, $\delta=-2\Gamma$.

These separate processes are shown more clearly in the SC-FPE results in Fig. 9. In Figs. 9(a) and 9(b) ($S=2$), the decelerating force dominates, but it is too weak to slow the initial distribution to within the narrow capture range of the Sisyphus force within the total elapsed time (1000τ). Figures 9(c) and 9(d) ($S=10$) show a regime where the force and diffusion act together to drive the atoms quickly and efficiently into the Sisyphus region. In Figs. 9(e) and 9(f) ($S=50$), $F(v)$ is larger so the capture time is less. However, here diffusion dominates: the initial velocity distribution broadens rapidly, a larger fraction of the atoms are lost before they reach the Sisyphus region, and the final velocity width is greater than for lower S. A more thorough analysis of this process, beyond the scope of the present work, would take into account the slope of the force vs velocity curve as well as $D(v)$ in the evolution of the width of the velocity distribution.

The functions $F(v)$ and $D(v)$ can be used to devise optimum strategies for beam collimation. For example, in Fig. 10 we show just $F(v)$ for two different detunings and a variety of intensities. The steep dispersion shape near $v=0$ arises from the lin$\perp$lin Sisyphus cooling, while the broader wings at higher velocity come from the Doppler cooling process. Collection of atoms at high velocity into a narrow cold peak is facilitated if there is not a gap in $F(v)$ between these two regimes. For $\delta=-3\Gamma/2$ [Fig. 10(a)], a deep minimum

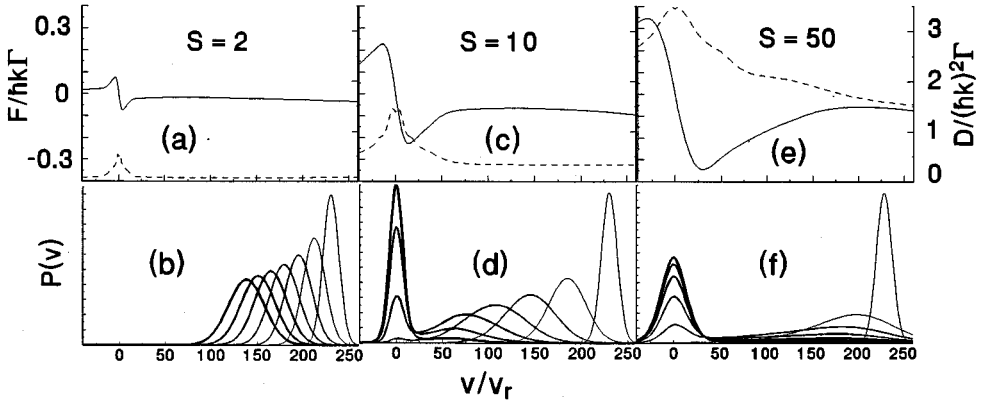

FIG. 9. Collection dynamics with semiclassical force and diffusion curves (top) for the ^{85}Rb $F=3\rightarrow4$ transition, with laser detuning $\delta=-3\Gamma/2$ and laser intensity (a), (b) $S=2$, (c), (d) $S=10$, and (e), (f) $S=50$. The initial velocity distribution is centered at $230v_r$ in each case, and the time evolution of $P(v)$ is shown in the three bottom graphs, for which the line thickness increases with elapsed time. In each case, the time steps are 600τ, and the final trace is for 3600τ.

in $|F(v)|$ occurs near $v=0.2\Gamma/k$ even for high laser intensity, so evidently the detuning is so large that high-velocity atoms would be stranded near this minimum and not make it into the Sisyphus region. On the other hand, for $\delta=-\Gamma/2$ [Fig. 10(b)], a modest laser intensity such as $S=5$ effectively removes the minimum. In addition, at smaller detuning the increased diffusion helps atoms through the gap region where the force is small. The optimum detuning is found to be close to $\delta=-\Gamma$, in good agreement with the empirical conclusions in Ref. [10].

C. Results with He* atoms

Our calculations and experiments on He* probe phenomena that are not easily observable in Rb or other heavy alkali-metal atoms because of their small value of ε. In Fig. 11, we show $E_{\rm av}$ and E_{ge} values from both AE [14] and QDM calculations to show these effects. Our AE calculations use a quantum basis but provide purely steady-state results,

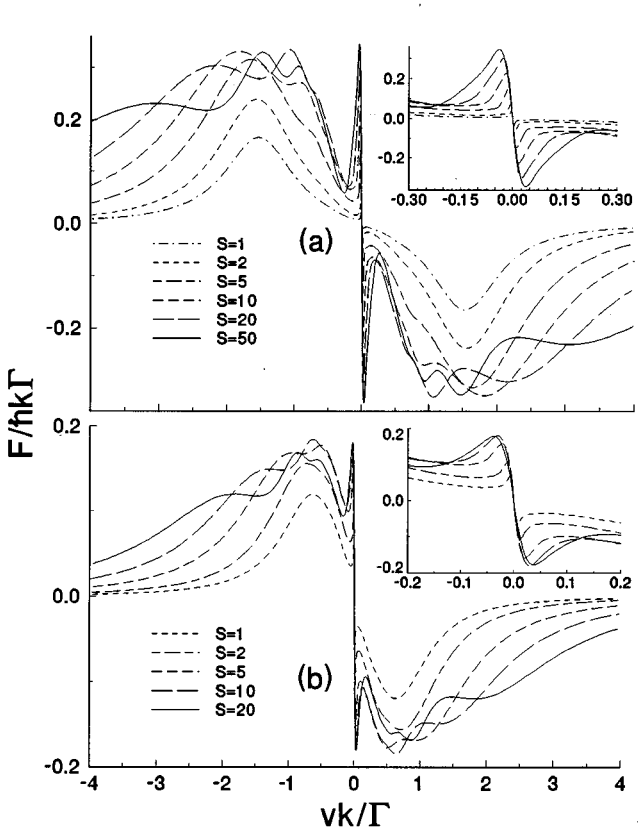

FIG. 10. Force vs velocity for several values of the saturation parameter S for a $J=3\rightarrow4$ transition. Insets show the low-velocity detail. (a) $\delta=-3\Gamma/2$. (b) $\delta=-\Gamma/2$.

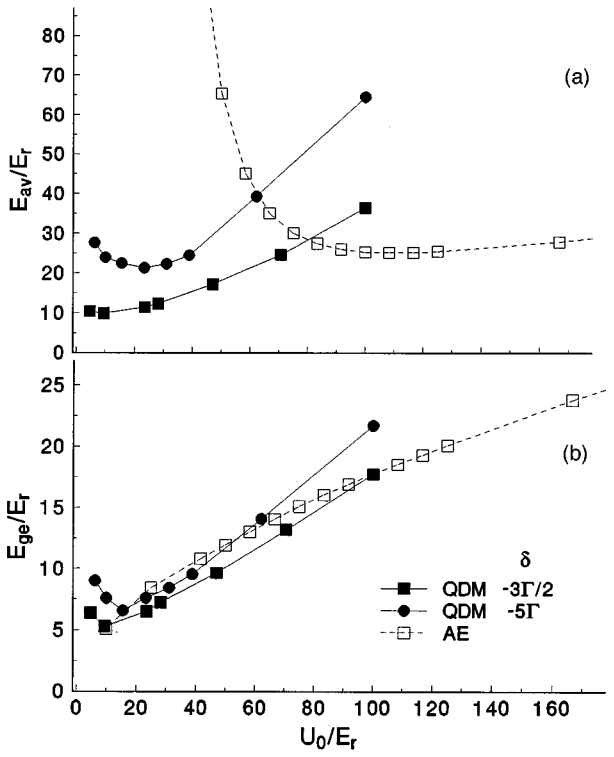

FIG. 11. Comparison of (a) $E_{\rm av}$ and (b) E_{ge} vs U_0/E_r for He* from QDM and AE calculations. Steady-state AE results depend on S, δ, and ε only through the parameter U_0/E_r.

whereas the QDM calculations are based on time evolution calculations starting with a distribution close to the steady-state value.

The AE results (no Doppler cooling) for $E_{\rm av}$ in Fig. 11(a) show the well-known minimum near $U_0/E_r \approx 100$ and the sharp rise at lower values. The results for $E_{\rm av}$ from QDM calculations show a lower minimum at a much lower value of U_0/E_r because Doppler cooling effects here collect atoms from the wings into the cold atom peak. For $U_0/E_r < 100$, Sisyphus cooling sharpens the velocity distribution at low $|v|$, hence E_{ge} decreases to a low value even in the AE results, which give much higher values for $E_{\rm av}$.

These plots of $E_{\rm av}$ and E_{ge} for He* reflect several consequences of the large value of ε in He*. First, the Sisyphus cooling limit for He* from AE calculations, $E_{\rm av} \approx 25E_r$ (the minimum kinetic energy for *any* detuning), is nearly four times the 1D Doppler limit of $7\hbar\Gamma/40 \approx 6.7E_r$ (which occurs with $\delta = -\Gamma/2$). For $\delta = -3\Gamma/2$ (-5Γ), the minimum value of $E_{\rm av}$ for Doppler cooling is about $11E_r$ $(34E_r)$, while for lin⊥lin cooling of He* from QDM calculations, the minimum value of $E_{\rm av}$ is $10E_r$ $(20E_r)$. By contrast, for Rb, the Sisyphus limit of $\approx 20E_r$ is much smaller than the Doppler limit (at $\delta = -\Gamma/2$) of $\approx 273E_r$. Thus for He*, the Doppler limit for $E_{\rm av}$ is comparable to the Sisyphus limit, suggesting that Doppler cooling plays a significant role in lin⊥lin cooling of He*. This is consistent with the conclusion one reaches from Fig. 11(a) that AE calculations of $E_{\rm av}$ are not reliable for He*.

This last conclusion appears to be inconsistent with the corresponding values of Γ_p/Γ and the standard estimates for the excited state fraction (exact for a two-level atom), $\Gamma_p/(2\Gamma_p+\Gamma)$. For lin⊥lin cooling of He* with $U_0/E_r = 20$, $\delta = -3\Gamma/2$ (-5Γ) and thus $S = 4.18(12.7)$, $\Gamma_p/\Gamma = 0.15$ (0.056). However, these values apply only to atoms with $v = 0$. For atoms close to the Doppler resonance velocity, $v_{\rm Dop} \approx \pm|\delta|/k$, Γ_p/Γ will be significantly larger. Since atoms with v near $v_{\rm Dop}$ play an important role in lin⊥lin cooling of He*, a large value of Γ_p/Γ here will invalidate AE calculations of $E_{\rm av}$ even though Γ_p/Γ is small for $v = 0$ atoms. The semiclassical approach also begins to be questionable for He* because typical values for v_{ge} for He* imply a violation of a key condition for the validity of the semiclassical approach, namely, $dP(v)/dv \ll P(v)/v_r$.

Another interesting feature of lin⊥lin cooling in He* is that the damping force region between the inner peaks of $F(v)$ at $|v| = \pm v_c$ is very much narrower than the steady-state Gaussian width v_{ge}, or that is, $v_{ge}/v_c \gg 1$. This contrasts with the case of heavier alkali metals for which v_{ge} is typically a few times v_c. Empirically we find for an $F = 1 \rightarrow 2$ transition in the low-intensity limit, $\overline{f} = v_c k/\Gamma_p = 0.13 + 0.03|\delta|/\Gamma$. (For an $F = 1/2 \rightarrow 3/2$ transition, $\overline{f} = 2/9$ independent of detuning [11], while for an $F = 3 \rightarrow 4$ transition, we find $\overline{f} \approx 0.045 + 0.014|\delta|/\Gamma$.) Letting $U_0/E_r = u$, from expressions given above and values of E_{ge} shown in Fig. 11, we obtain $v_{ge}/v_c \approx 1.34 + 71/u$ for $\delta = -3\Gamma/2$, and $v_{ge}/v_c \approx 1 + 162/u$ for $\delta = -5\Gamma$. For $u = 100$ as for Rb, v_{ge}/v_c is thus in the range 2–3, while for $u = 10 - 30$, as is of interest for He* (Fig. 11), $v_{ge}/v_c \approx 5 - 20$. The work described here is a systematic study of this unusual situation in which the Doppler cooling limit is comparable to the minimum obtained with ''sub-Doppler'' methods, and where the steady-state width of the velocity distribution substantially exceeds the lin⊥lin peak-to-peak separation of $F(v)$ even under near optimum conditions.

Our measurements exhibit the effects of Doppler cooling in the velocity distributions, but the interpretation requires some care because of non-steady-state effects. Non-Gaussian shapes can occur when cooling is incomplete and a narrow cool atom peak lies on top of the broader initial distribution. As the atoms traverse the laser's spatial distribution, they see the light intensity vary as a Gaussian with a FWHM of about $10\ \mu s \approx 100\tau$. The short interaction time allows remnants of the initial velocity distribution (Gaussian with a FWHM of about $20v_r$) to persist at low intensities or large detunings.

At relatively high laser intensity, however, where the optical pumping rate Γ_p is rapid and the cooling reaches steady state, a broad pedestal does appear in the observed $P(v)$ which can be associated with the Doppler part of the cooling process. This is seen in Figs. 12(a) and 12(e), where measurements were made with the laser profile cutoff at 85% of its peak value, for $S = 32$.

We also studied equilibration of the He* $P(v)$ to lower intensity laser light in the Gaussian tail of the laser beam profile by unblocking the downstream side of the laser beam. Experimental results are shown on the left side of Fig. 12, and computational results are presented in Fig. 13. The additional narrowing in our experimental data is apparent in the right plot in each pair in Fig. 12. The plot on the upper right of Fig. 13 shows the laser intensity affecting an atom vs time, with and without a cutoff at about 85% maximum intensity. For the calculations in this plot we have included the intensity profile of the laser beam in our QDM model by introducing a temporal variation of light intensity as the atoms move through the laser beam. The temporal evolution of the velocity distributions shown in this figure shows additional narrowing in the low-intensity region downstream when the Gaussian tail of the laser is *not* cut off.

V. DISCUSSION OF RESULTS, AND CONCLUSIONS

Our results, together with previous reports [8–10,30], present encouraging possibilities for the practical production of bright thermal atomic beams (see also a brief discussion in [40]). A large capture range and high cooling rate combine to make high-intensity cooling useful as a preliminary step in beam collimation. The velocity capture range can be further enhanced by tilting the transverse laser cooling beam [41,42]. Even brighter beams can easily be achieved by following an optimized region of high intensity with a sufficiently long low-intensity tail to permit an equilibration to a cold peak of minimal velocity width [29]. Following this, one could also contemplate a region optimized for velocity selective coherent population trapping (for He*) or bichromatic velocity selective coherent population trapping [43] (for Rb) to produce even narrower velocity distributions. Two-dimensional magneto-optic traps, consisting of quadrupole magnetic fields plus transverse cooling lasers, have been used to spatially concentrate an atomic beam after a narrow transverse velocity distribution has been achieved [44,45,41,42,46]. Other schemes to optimize sub-Doppler and subrecoil cooling separately have been proposed [47],

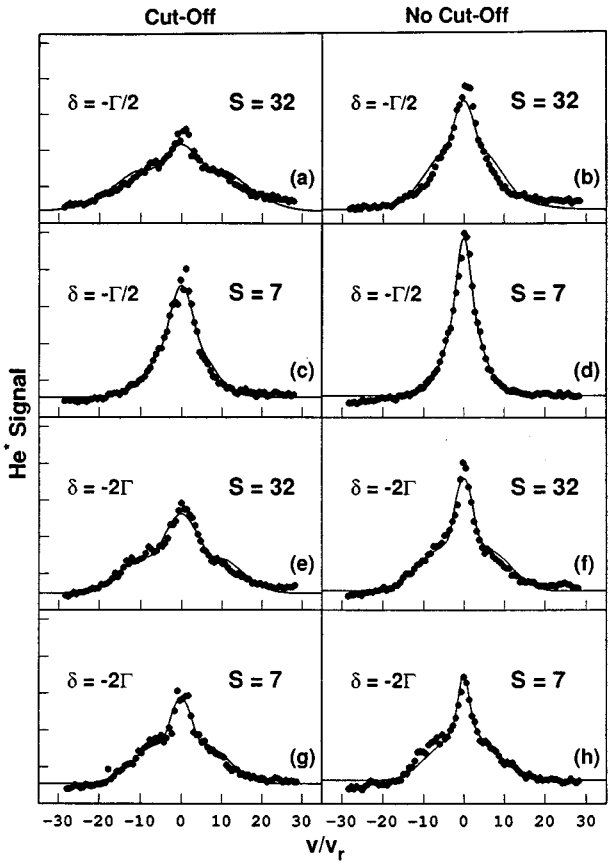

FIG. 12. Measured velocity profiles for He*. (a), (c), (e), (g) are taken with the 85% cutoff in place. (b), (d), (f), (h) are for the full 32 mm aperture and show narrowing due to equilibration to lower intensity in the tail of the laser spatial distribution. (a), (e) for $S=32$ clearly exhibit the narrow peak atop a broader pedestal due to Doppler cooling. (c), (d), (g), (h) on the other hand have not yet reached steady state, and the pedestal is due to the initial distribution.

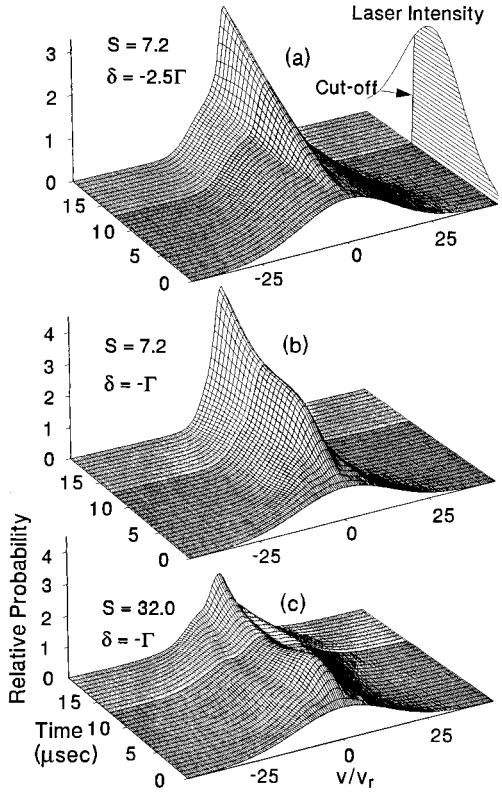

FIG. 13. Calculated evolution of the velocity distribution of He* atoms for three parameter ranges: (a) $S=7.2$, $\delta=-5\Gamma/2$, (b) $S=7.2$, $\delta=-\Gamma$. (c) $S=32$, $\delta=-\Gamma$.

and it has also been found that subrecoil and Sisyphus cooling can coexist [48], creating brighter subrecoil beams in the high-intensity regime [4].

Our experimental results demonstrate that with higher laser intensity, more atoms can be collected into the cold peak while at the same time the FWHM increases by a relatively small amount. To establish some of the systematics in this regime, we have compared our measurements to results from both QDM and SC calculations. High laser intensities and small detunings require that excited states not be eliminated from the calculations. Semiclassical calculations using $F(v)$ and $D(v)$ functions obtained with excited states included give useful if not quantitative accuracy for $F_g>1$. These functions are useful in understanding the cooling dynamics in different regimes and thus in devising optimal experimental strategies.

Our experimental results for He* and many computational results show that in the high-intensity regime, velocity distributions are typically non-Gaussian in shape. There are two velocity regimes: one associated with the steep force function near $v=0$ from Sisyphus cooling and one with the less steep Doppler force which extends to higher velocities. Doppler cooling can greatly increase the velocity capture range, and becomes more significant for light atoms (large ε) such as He*. The optimum detuning is determined from the desire to maximize the capture velocity while avoiding a gap in $F(v)$ between the region of large Doppler force and the Sisyphus region, and is found to be approximately $\delta=-\Gamma$, in agreement with other studies [10]. He* represents an interesting, previously unstudied regime, where the Doppler temperature is lower than the mimimum predicted by AE calculations of the Sisyphus cooling. We plan to explore this recoil dominated regime further by using the $2\,^3S_1\rightarrow 3\,^3P_2$ transition in He* at 389 nm.

ACKNOWLEDGMENTS

This work was supported by the National Science Foundation, the Office of Naval Research, and by a grant of computer time from the Cornell Theory Center. We are indebted to M. R. Doery and E. J. D. Vredenbregt for the adiabatic elimination results and for valuable discussions.

[1] A. Aspect, E. Arimondo, R. Kaiser, N. Vansteenkiste, and C. Cohen-Tannoudji, Phys. Rev. Lett. **61**, 826 (1988).
[2] J. Lawall, F. Bardou, B. Saubamea, K. Shimizu, M. Leduc, A. Aspect, and C. Cohen-Tannoudji, Phys. Rev. Lett. **73**, 1915 (1994).
[3] J. Lawall, S. Kulin, B. Saubamea, N. Bigelow, M. Leduc, and C. Cohen-Tannoudji, Phys. Rev. Lett. **75**, 4194 (1995).
[4] M. Widmer, M. J. Bellanca, W. Buell, H. Metcalf, M. Doery, and E. Vredenbregt, Opt. Lett. **21**, 606 (1996).
[5] H. F. Hess, Phys. Rev. B **34**, 3476 (1986).
[6] W. Petrich, M. H. Anderson, J. R. Ensher, and E. A. Cornell, Phys. Rev. Lett. **74**, 3352 (1995).
[7] K. B. Davis, M.-O. Mewes, M. R. Andrews, N. J. van Druten, D. S. Durfee, D. M. Kurn, and W. Ketterle, Phys. Rev. Lett. **75**, 3969 (1995).
[8] M. R. Williams, C. Xie, W. F. Buell, T. Bergeman, and H. Metcalf, *Coherence and Quantum Optics VII*, edited by J. Eberly, L. Mandel, and E. Wolf (Plenum, New York, 1996), p. 377.
[9] D. Milic, M. D. Hoogerland, K. G. H. Baldwin, and R. E. Scholten, Quantum Semiclassic. Opt. **8**, 629 (1996).
[10] R. Scholten, R. Gupta, J. McClelland, R. Celotta, M. S. Levenson, and M. G. Vangel, Phys. Rev. A **55**, 1331 (1997).
[11] J. Dalibard and C. Cohen-Tannoudji, J. Opt. Soc. Am. B **6**, 2023 (1989).
[12] Y. Castin, J. Dalibard, and C. Cohen-Tannoudji, in *Light Induced Kinetic Effects on Atoms, Ions and Molecules*, Proceedings of the Workshop, Held in Marciana Marina, Elba Island, Italy, 1990, edited by Luigi Moi *et al.* (ETS Editrice, Pisa, 1991).
[13] Y. Castin and J. Dalibard, Europhys. Lett. **14**, 761 (1991).
[14] M. R. Doery, Ph.D. dissertation, SUNY at Stony Brook, Stony Brook, New York, 1995.
[15] K. Berg-Sørensen, Y. Castin, E. Bonderup, and K. Mølmer, J. Phys. B **25**, 4195 (1992).
[16] C. Xie, Ph.D. dissertation, SUNY at Stony Brook, Stony Brook, New York, 1995.
[17] C. Xie and T. Bergeman, Bull. Am. Phys. Soc. **40**, 4 (1995).
[18] C. Xie, M. R. Doery, and T. Bergeman (unpublished).
[19] C. Salomon, J. Dalibard, W. D. Phillips, A. Clairon, and S. Guellati, Europhys. Lett. **12**, 683 (1990).
[20] W. Itano and D. Wineland, Phys. Rev. A **25**, 35 (1982).
[21] R. J. Cook, Phys. Rev. A **22**, 1078 (1980).
[22] M. R. Doery, E. J. D. Vredenbregt, and T. Bergeman, Phys. Rev. A **51**, 4881 (1995). In Eq. (37) of this paper, $s/3$ should be replaced by s/L and 2/5 should be replaced by $(\hbar k)^2\Gamma/10$.
[23] G. Nienhuis, P. van der Straten, and S.-Q. Shang, Phys. Rev. A **44**, 462 (1991).
[24] H. Risken, *The Fokker-Planck Equation, Methods of Solution and Application* (Springer-Verlag, Berlin, 1984), Chap. 9.
[25] V. G. Minogin, Zh. Éksp. Teor. Fiz. **80**, 2231 (1981) [Sov. Phys. JETP **53**, 1164 (1981)].
[26] B. Matisov, E. Korsunsky, E. Gordienko, and L. Windholz, Laser Phys. **4**, 835 (1994).
[27] E. Korsunsky, A. Snegiriov, B. Matisov, and L. Windholz, Z. Phys. D **30**, 23 (1994).
[28] K. Mølmer, J. Phys. B **27**, 1889 (1994).
[29] J. Chen, J. G. Story, J. J. Tollet, and R. G. Hulet, Phys. Rev. Lett. **69**, 1344 (1992).
[30] M. D. Hoogerland, J. P. J. Driessen, E. J. D. Vredenbregt, H. J. L. Megens, M. P. Schuwer, H. C. W. Beijerinck, and K. A. H. vanLeeuwen, Appl. Phys. B: Lasers Opt. **62**, 323 (1996).
[31] J. Javanainen, Phys. Rev. A **44**, 5857 (1991).
[32] T. Bergeman, Phys. Rev. A **48**, R3425 (1994).
[33] O. Nilsson, S. Saito, and Y. Yamamoto, Electron. Lett. **17**, 589 (1981).
[34] M. R. Doery, M. T. Widmer, M. J. Bellanca, W. F. Buell, T. H. Bergeman, H. J. Metcalf, and E. J. D. Vredenbregt, Phys. Rev. A **52**, 2295 (1995).
[35] T. Chuang and H. Metcalf, Appl. Opt. **30**, 2495 (1991).
[36] J.-Y. Courtois, Ph.D. thesis, École Normale Supérieure, Paris, 1993.
[37] J. M. Sancho, M. San Miguel, S. L. Katz, and J. D. Gunton, Phys. Rev. A **26**, 1589 (1982).
[38] H. Dekker, Phys. Lett. **90A**, 26 (1982).
[39] V. Dunjko, S. Hatamian, and T. Bergeman, Bull. Am. Phys. Soc. **48**, 1075 (1996).
[40] H. Metcalf and P. van der Straten, Phys. Rep. **244**, 203 (1994).
[41] E. J. D. Vredenbregt, K. A. H. van Leeuwen, and H. C. W. Beijerinck, Opt. Commun. (to be published).
[42] P. van der Straten (private communication).
[43] M. R. Doery, R. Gupta, T. Bergeman, H. Metcalf, and E. J. D. Vredenbregt, Phys. Rev. A **51**, 2334 (1995).
[44] E. Riis, D. Wiess, K. Moler, and S. Chu, Phys. Rev. Lett. **64**, 1658 (1990).
[45] J. Nelleson, J. Werner, and W. Ertmer, Opt. Commun. **78**, 300 (1990).
[46] J. Weiner (private communication).
[47] P. Marte, R. Dum, R. Taïeb, P. Zoller, M. S. Shahriar, and M. Prentiss, Phys. Rev. A **49**, 4826 (1994).
[48] M. S. Shahriar, P. R. Hemmer, M. G. Prentiss, P. Marte, J. Mervis, D. P. Katz, N. P. Bigelow, and T. Cai, Phys. Rev. A **48**, R4035 (1993).